Indian Journal of Chemistry
Vol. 62, June 2023, pp. 618-626
DOI: 10.56042/ijc.v62i6.2527

# Enhanced photoactivity effect of Ag metal loading on $Zr^{4+}$ doped N-$TiO_2$ obtained by microwave assisted method

Rohant Dhabbe[a], Vinayak Gawade[a,b], Kabir Kumbhar[a], Sandip Sabale*[a] & Kalyanrao Garadkar*[b]

[a] Department of Chemistry, Jaysingpur College, Jaysingpur 416 101, India

[b] Department of Chemistry, Shivaji University, Kolhapur 416 004, India

E-mail: srsabale@gmail.com, kmg_chem@unishivaji.ac.in

*Received 05 August 2022; accepted(revised) 19 May 2023*

Herein, we report the fabrication of Ag metal loading on Zr-doped-N-$TiO_2$ (AgZrT) nanocomposites (NCs) *via* microwave-assisted impregnation reduction method. The main objective of the work is to study the effect of Ag loading on structural, chemical and photoactivity of Zr-doped-N-$TiO_2$(ZrT). The obtained NCs were characterized using XRD, HRTEM, EDS, XPS *etc*. Obtained AgZrT NCs showed the existence of metastable anatase phase with an average crystallite size of about 10 nm supported by HRTEM. The presence of Ti, Zr and Ag is confirmed by EDS while the metallic state of Ag and oxidation state of Ti and Zr (+4) is confirmed by using XPS. The Ag loading effect on photoactivity of ZrT NPs was studied under UV and direct sunlight using model dye Methyl Orange (MO). The positive impact of Ag metal loading is supported by the enhanced photoactivity of ZrT. The degradation kinetics for MO and its plausible mechanism under sunlight is proposed.

**Keywords**: Ag loaded -ZrNT$iO_2$, Structural Characterization, Microwave assisted synthesis, Photoactivity, Methyl Orange

Nanomaterials with diversified physicochemical properties have potential applications including but not limited to nanomedicine, biomedical sciences, engineering, environmental remediation especially waste water treatment[1]. Wastewater from various industries, manufacturing plants, laboratories contains many contaminants such as reactive azo dye, hetero atom containing pesticides *etc*., which causes severe environment issues[2]. Hence the research was focused on the removal of organic pollutants mainly organic and hazardous dyes contaminated from wastewater due to its hazardous facts[3, 4]. Photocatalysis have paid much more attention for the degradation of such reactive dye pollutants because of their unique properties and potential applications in all areas of science[5–7] and semiconductor catalyzed degradation of dye is nowadays most utilized photocatalysis technique employed for degradation of organic contaminants[8] termed as heterogeneous photocatalysis. Accordingly, the research has turned towards heterogeneous photocatalysis, which uses metal oxides or mixed metal oxide semiconductors such as $TiO_2$,$SnO_2$, $ZrO_2$, $Co_{0.5}Cu_{0.5}Fe_2O_4$, *etc*[9–12].

Semiconductor photocatalysis is considered one of the best strategies for dealing with the energy crisis and pollution. In particular, nanocrystalline $TiO_2$ is the most promising semiconductor photocatalyst for dye treatment due to possession of specific chemical and physical properties, high photo corrosion resistance, easy accessibility, non-toxicity and cost effectiveness[13–15]. However, virgin $TiO_2$ have band gap 3.0-3.7 eV, which limits its activity in UV region[16,17]. Likewise, the recombination rate of photogenerated electron ($e^-$)-hole ($h^+$) pairs is also high which promotes low quantum efficiency. These stated characteristics limit its application as photocatalyst in visible region. There are several modifying strategies used to adjust the band gap of $TiO_2$ towards the visible region by doping of noble metals like Ag, Au, Pt, Pd *etc*. ions (cations, anions *etc*.) and non-metals like N, S *etc*.[18]. Non-metal doping such as nitrogen (N) enhances the visible light absorbability by narrowing the band-gap of $TiO_2$, although the electron-hole pair's recombination rate is higher.

Among the potential solids, zirconium (Zr) has attracted attention owing to its exceptional ceramic properties but also its excellent mechanical properties, long-term conductivity, and stability. The Zr doping in $TiO_2$ will result in enhancement of many ideal properties of photocatalyst such as stability of anatase phase with inhibition of recombination centers and

shift of absorption towards visible region[19–21]. In addition, photocatalysis using $TiO_2$ or doped $TiO_2$ was performed under UV light. Therefore, an attempt has been made to develop highly advantageous photocatalyst that can restrain the electron hole pair recombination and can utilize visible light for photocatalysis.

Considering the above discussion, we report herewith fabrication of Zr doped N-$TiO_2$ nanoparticles by easy, rapid, energy efficient microwave assisted method and its modification with Ag by impregnation-reduction method. This Ag loaded Zr-N-$TiO_2$ nanocomposites [AgZrT NCs] were further investigated for photodegradation of methyl orange under UV and natural sunlight. The degradation kinetics and plausible pathway along with LC-MS of degraded products are reported and discussed.

## Experimental Section

### Chemicals

Tetra-Isopropyl Titanate (TTIP, 98%), surfactant Cetyltrimethylammonium Bromide (CTAB, 99%) were bought from Spectrochem Pvt. Ltd., Mumbai (India). Zirconium oxychloride procured from Himedia Lab Pvt. Ltd., Mumbai. Aqueous Ammonia (25% purity) was obtained from Loba Chemie Pvt. Ltd., Mumbai (India). Silver nitrate ($AgNO_3$) was procured from Merck, Mumbai. From Changshu Yangquan Chemicals (China) we purchased Absolute ethanol (99.9%) and from Thomas Baker Pvt. Ltd. (Mumbai) we procured Sodium dodecyl sulfate (SDS, extrapure). Millipore water obtained from millipore water system (Millipore Corp. Bangalore, India) used for all experiments and washing purposes.

### Fabrication of microwave assisted Zr doped N-$TiO_2$ nanoparticles

Zr doped $TiO_2$ powder was fabricated as per our previous report[22]. Briefly, controlled addition of 0.1 M titanium tetra-isopropoxide (TTIP) in 0.1 L ethanol (absolute) was carried out. For the fabrication of different mole % of Zr (Zr-T1 to Zr-T3 represents 0.25, 0.5, 0.75 mol% Zr in N-$TiO_2$) calculated amount of zirconium oxychloride is added. Then sufficient amount of mixed surfactant solution (1% CTAB + 1% SDS) was carefully added and ammonia addition continued till *p*H=8. After complete precipitation washing with millipore water and acetone for several times were done. The washed precipitate was subjected to microwave irradiation with on-off cycle from 20 on - 40 s off in domestic microwave oven having specific parameters of wattage and frequency (900 W/250 MHz). The dried precipitate was further calcined in muffle furnace (250 ° C / 3 h).

### Synthesis of AgZrTNCs

Ag loaded Zr doped anatase N-$TiO_2$ fabricated by microwave method was further improved with silver nanoparticles (NPs) using impregnation-reduction method. Synthesized Zr doped N-$TiO_2$ powder having optimum content of Zr (0.5 mol% of Zr) mixed in 0.02 L water with sonication. For synthesis of different wt% of Ag (0.1 to 0.75) loading, pre calculated amount of Ag source (silver nitrate) was added in above mixture stirred for 1 hr to get of $Ag^+$ and Zr doped N-$TiO_2$ in solution. $Ag^+$reduction was done using sodium borohydride solution. The prepared AgZr-N-$TiO_2$NCs was dried (120°C /60 min) to eliminate water and denoted as AgZrT1, AgZrT2, AgZrT3 and AgZrT4 for different Ag content of 0.1, 0.25, 0.50 and 0.75 wt% respectively.

### Characterization of AgZrTNCs

Powder XRD patterns of AgZrT NCs catalysts were acquired using a Panalytical X-ray diffractometer fitted with Cu Kα as source radiation (λ=1.5406 Å at 40 kV) in the range of 2θ, 10 to 90°. The structural related information and size of the synthesized materials were acquired using TEM, JEOL 3010. FT-IR was taken using a Perkin−Elmer spectrometer (BX-II). EDS spectra and mapping were recorded using JEOL-6360. The diffused reflectance was obtained on UV-Vis NIR spectrophotometer (Varian Cary-5000).

### Catalytic activity of AgZrTNCs under light.

The photo activity of AgZrTNCs was investigated for the degradation of methyl orange (MO) by using ordinary sunlight and simulated UV light (365 nm). Optimization of catalyst for the degradation MO (20 ppm) was carried out using 0.5 to 2.0 g/$dm^3$ of catalytic amount in open air under sunlight. Typically, photoreactor containing 0.1 L of 20 ppm MO was stirred in the dark to confirm the adsorption-desorption equilibrium, followed by exposure under natural sunlight. All photodegradation experiments were done at ambient condition of temperature. At a specific time, sample solutions were collected from photoreactor and the NCs were separated using centrifugation. The MO concentration was recorded using Shimadzu UV-VIS spectrophotometer bearing Model-UV-3600.

## Results and discussion

### Structural and optical properties

The XRD study was carried out for phase confirmation of Zr doped N-$TiO_2$ nanomaterial. The imperfect crystallinity was observed in case of low calcination temperature; therefore, the materials were calcined from 150 to 250°C[23]. At 250°C, most intense crystalline peaks were observed in XRD pattern of Zr-N$TiO_2$ compared to 150°C and 200°C, therefore 250°C was elected as optimized temperature of calcination as shown in Fig. 1A. For different wt% Ag, x-ray diffraction data confirms that there is formation of crystalline structure having anatase phase with tetragonal crystal system (JCPDS card No. 01-084-1286) having diffraction peaks at 25.2° (101), 37.84° (004), 47.84° (200), 62.8° (204) and 75.34° (215) (Fig. 1A). Despite the variation in Ag loading (0.1 to 0.75 wt%), the crystalline phase of NCs was found to be anatase $TiO_2$. Hence, the loading of Ag at such low content did not significantly affect the crystalline state of NCs. Major peak for Zr doped N-$TiO_2$ found to be almost same for AgZrTNCs, except the changes in intensity. The nonappearance of Ag peak in the XRD data is attributed to low content and high dispersion of Ag NPs on the outersurface of the Zr doped N-$TiO_2$. The average crystallite size was evaluated by Debye Scherrer's equation[22].

$$D = (0.9\lambda/\beta \cos\theta) \quad \ldots (1)$$

where, crystallite size (D) depends upon wavelength of X-ray ($\lambda$) and $\beta$ is full width at half maximum (FWHM). The NCs crystallite sizes were found around 8-10 nm as given in Table 1 including lattice parameters (a/b/c) and cell volume.

FT-IR spectra of AgZrT3 NC (Fig. 1B), shows bands at 3471-3200 $cm^{-1}$ and 1624 $cm^{-1}$ were

Table 1 — Crystallographic data (lattice parameter and volume) of obtained NCs determined considering $TiO_2$ in anatase phase having tetragonal crystal structure

| NC | Lattice parameter (Å) | | Volume ($a^2c$) ($Å)^3$ | Crystallite size (nm) |
|---|---|---|---|---|
| | (a=b) | (c) | | |
| AgZrT1 | 3.8027 | 9.5271 | 137.77 | 8.85 |
| AgZrT2 | 3.8016 | 9.5166 | 137.53 | 9.89 |
| AgZrT3 | 3.8052 | 9.5440 | 138.18 | 9.96 |
| AgZrT4 | 3.7944 | 9.4979 | 136.74 | 10.02 |

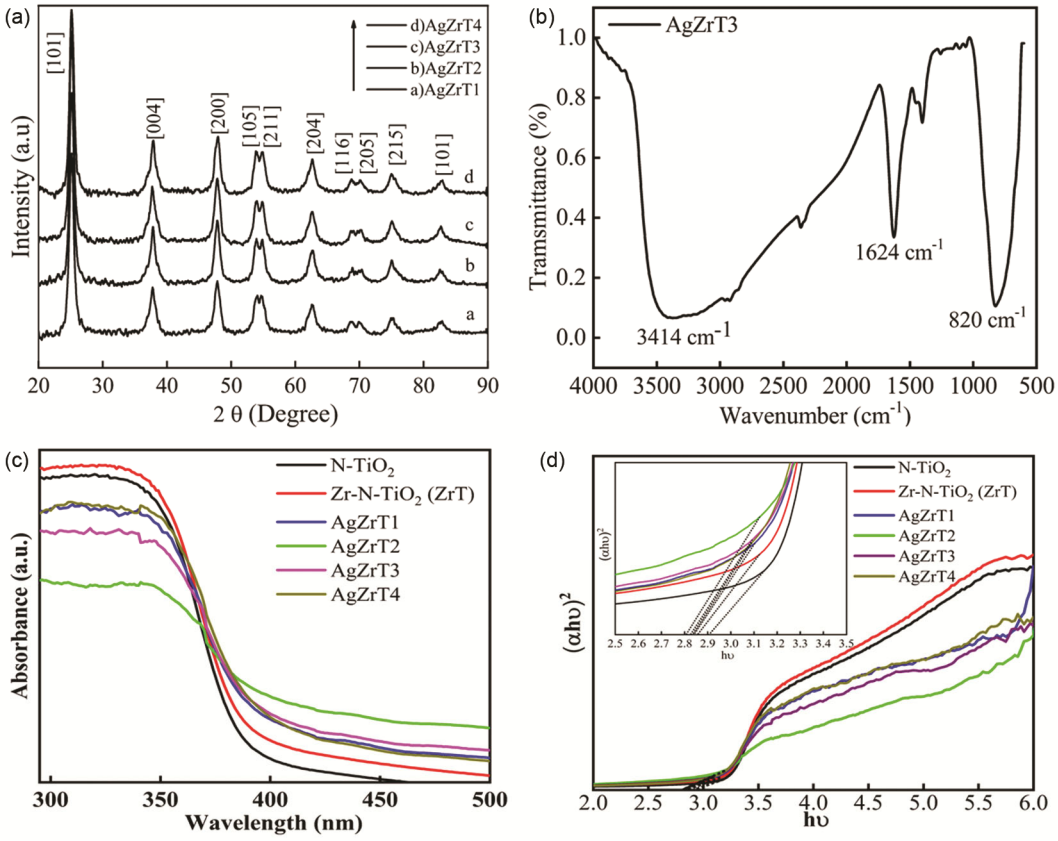


Fig. 1 — A) XRD; B) FTIR spectrum; C) DR-UV spectra and D) Tauc plot of Ag loaded Zr doped N-$TiO_2$ where (a) AgZrT1 (0.1 wt%Ag); b) AgZrT2 (0.25 wt %); c) AgZrT3 (0.5 wt %); d) AgZrT4 (0.75 wt %).

observed owing to -OH group from adsorbed water on the $TiO_2$ and may play key role in photoactivity. The wide peak at 850-670 $cm^{-1}$ is the characteristic peak of Metal-oxygen bonding (Ti-O) which confirms the formation of metal oxygen bonding[24].

The band gap values (Eg) is a crucial factor for the normal photocatalytic applications. The UV-Vis DRS spectra of AgZrTNCs are shown in Fig. 1C. The shift in absorbance towards the visible region was probably due to Ag NPs[25]. The relationship between coefficient of absorption and the photon energy were obtained from Tauc equation.

$$(\alpha h\nu) = A\,(h\nu - Eg)^n \quad \ldots (2)$$

where, the absorption coefficient (α) depends upon frequency(ν), proportionality constant (A) and band gap energy values (Eg). In the above equation 'n' decides the type of transition of semiconductors which is direct in case of $TiO_2$[26] and for the sake of calculations, n = 0.5 is used in equation (2). Band gap values show gradual decrease with increase in Ag content from 2.91 to 2.81 eV for 0.1 to 0.75 wt% respectively (Fig. 1D). The decrease in band gap from 2.86 eV (Zr-N-$TiO_2$) from our previous report[23] to the value of 2.81 eV is due to loading of Ag.

**Compositional and morphological properties**

The EDS spectra play role in material identification and composition of NCs. The EDs spectra along with elemental mapping of AgZrT3 NC were recorded for the confirmation as given in Fig. 2. EDS spectra shows the presence of elements Ti, N, O, Zr and Ag at 4.508, 0.392, 0.525, 2.145 and 2.987 keV respectively. The Wt % of Ti, O, Zr, Ag and N from EDS data is found to be 51.9%, 43.2%, 3.3%, 1.1% and 0.5% respectively which confirms the formation of AgZrT3 NC.

The oxidation state and chemical environment of different elements such as Zr, Ti, O, N and Ag in AgZrT3 NC was determined by XPS analysis and its survey spectrum as shown in Fig. 3A. From XPS data binding energy values for Ti were well deconvoluted by two curves due to spin–orbit components ($^2p_{3/2}$ and $^2p_{1/2}$) and reported at 458.8 eV and 464.5 eV and

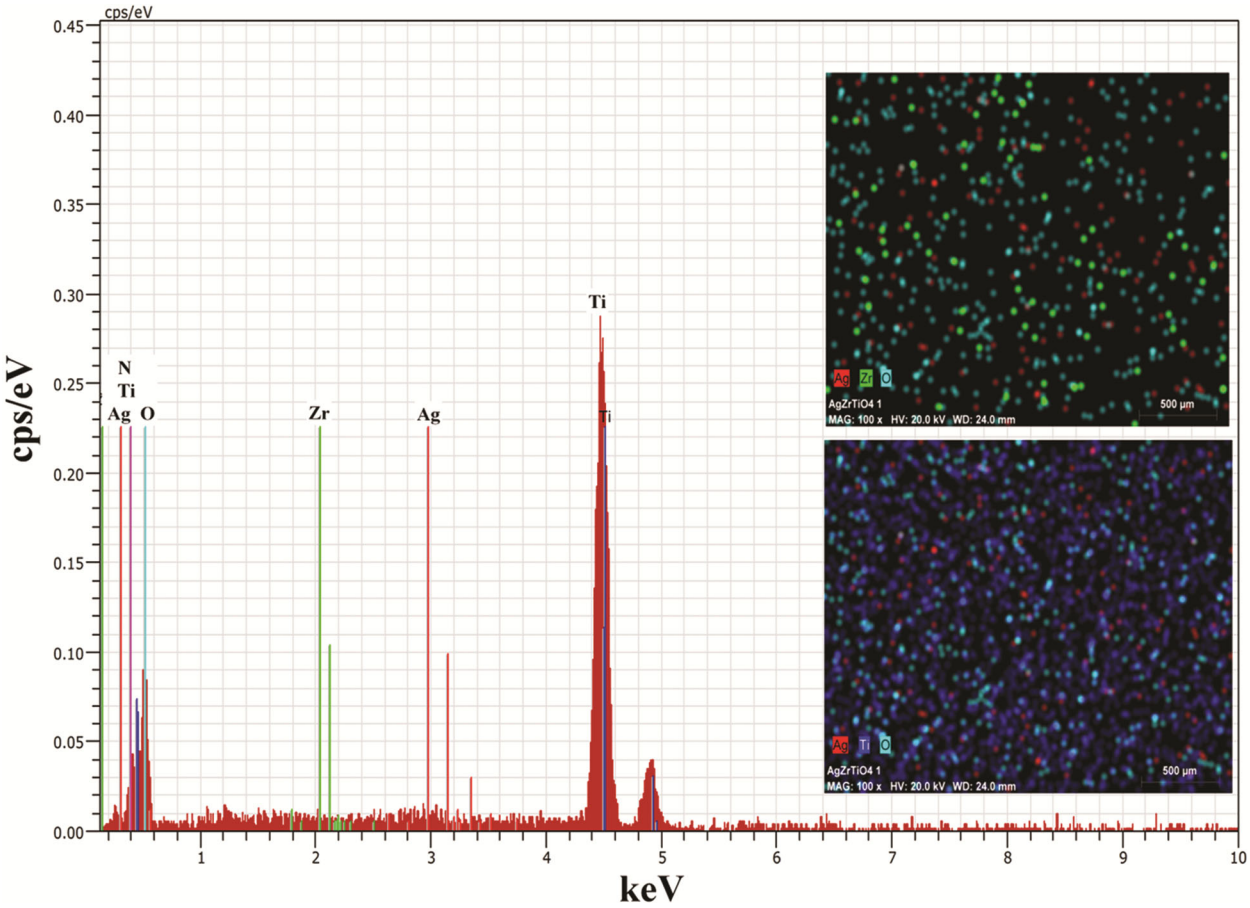


Fig. 2 — Energy dispersive X-ray spectra and elemental mapping of Ag loaded Zr doped N-$TiO_2$

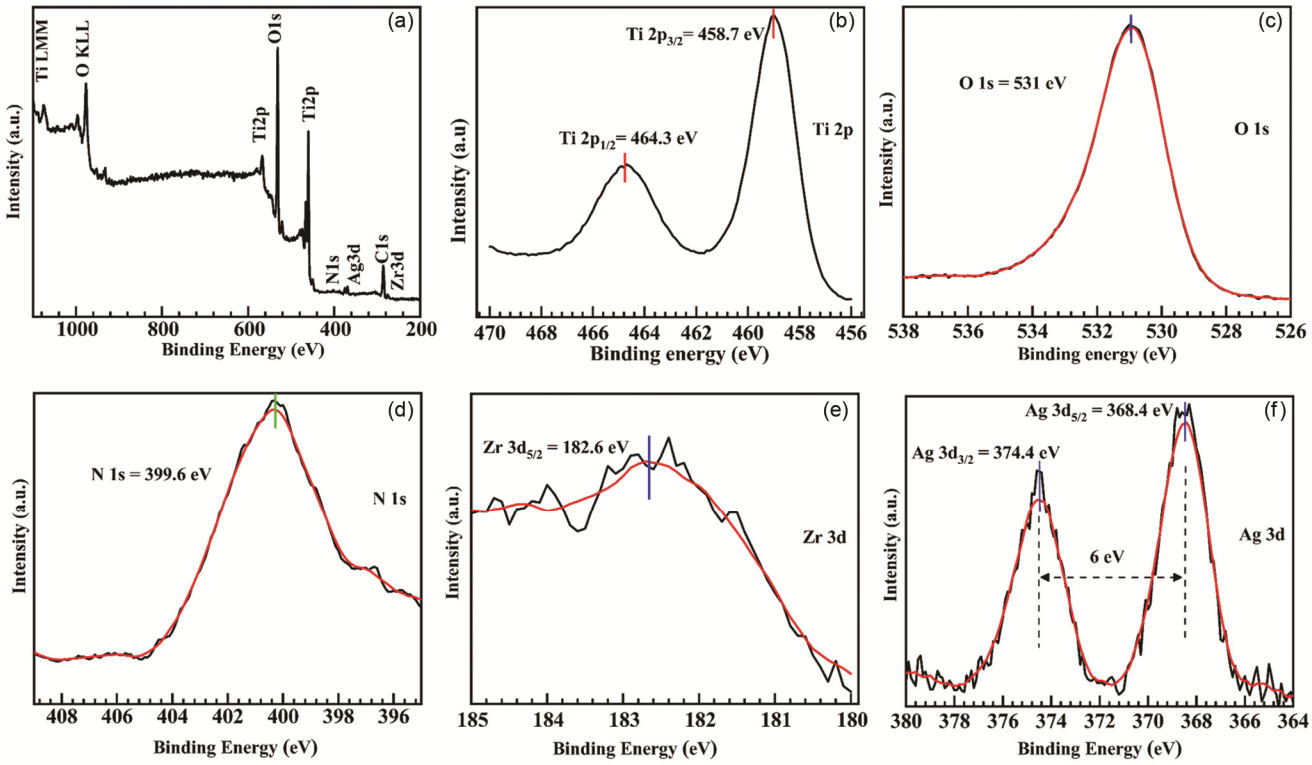


Fig. 3 — X-Ray photoelectron spectroscopy spectra of Ag loaded Zr doped N-$TiO_2$ NC A) the survey spectrum and XPS core spectra of B) Ti 2p, C) O 1s, D) N 1s, E) Zr 3d, F) Ag 3d.

confirms the Ti element in $Ti^{4+}$state[27]. In case of AgZrT3 NC, the binding energy values for Ti centered at 458.7 eV ($^2p_{3/2}$) and 464.3 eV ($^2p_{1/2}$) is shown in Fig. 3B. The XPS data of the O 1s is shown in Fig. 3C having binding energy value at 531 eV whereas, N1s core level spectra was observed at 399.6 eV (Fig. 3D) in the AgZrT3[28]. Fig. 3E shows that the binding energy value of Zr is centered at 182.6 eV which confirms Zr in +4 oxidation state. The binding energy value of Ag $3d_{5/2}$ is found to be at 368.4 eV and Ag $3d_{3/2}$ is centered at around 374.4 eV (Fig. 3F). It is observed that the binding energy difference between the Ag peaks is around 6 eV which indicate that silver is in pure metallic and with zero oxidation state[29].

The crystal morphologyand formation of AgZrT3 NC was confirmed by TEM which reveals the NCs with a narrow size distribution (Fig. 4A). The dark spots on the outer surface of AgZrT3NC in TEM images were observed due to higher electron density of silver than Zr-$TiO_2$. The average size around 8 to 10 nm for fabricated NC was observed which is in good correlation with XRD results (Fig. 1A). Distinct lattice fringes seen in HR-TEM which is presented in Fig. 4B indicating d spacing of 0.35 nm for $TiO_2$

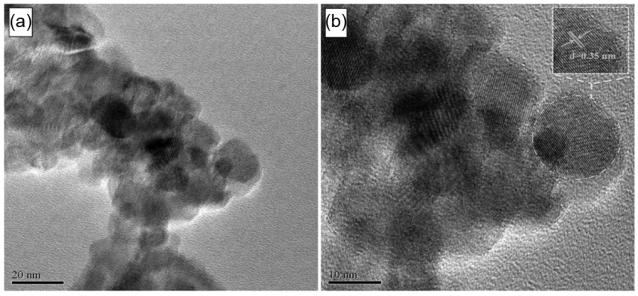


Fig. 4 — TEM image of A) AgZrT3 B) HRTEM image of AgZrT3 (inset showing d=0. 35 nm)

(101) plane which again form good correlation with XRD results.

**Factors affecting photocatalytic degradation of MO dye**

**Effect of Ag Content in Zr-N-$TiO_2$**

The kinetics model used for investigating rate constant and order for the photodegradation of MO is Langmuir-Hinshelwood and rate equation used for the same is given as, $\ln (C_0/C) = kt$[30, 31]. Fig. 5A shows the linear relationship between $\ln(C_0/C)$ *vs* time (t) for the photocatalytic reaction which follows the pseudo-first order kinetics for low content of Ag. With gradual increment in Ag concentration from 0.1 to 0.5 wt %, the rate constant values gradually increase from

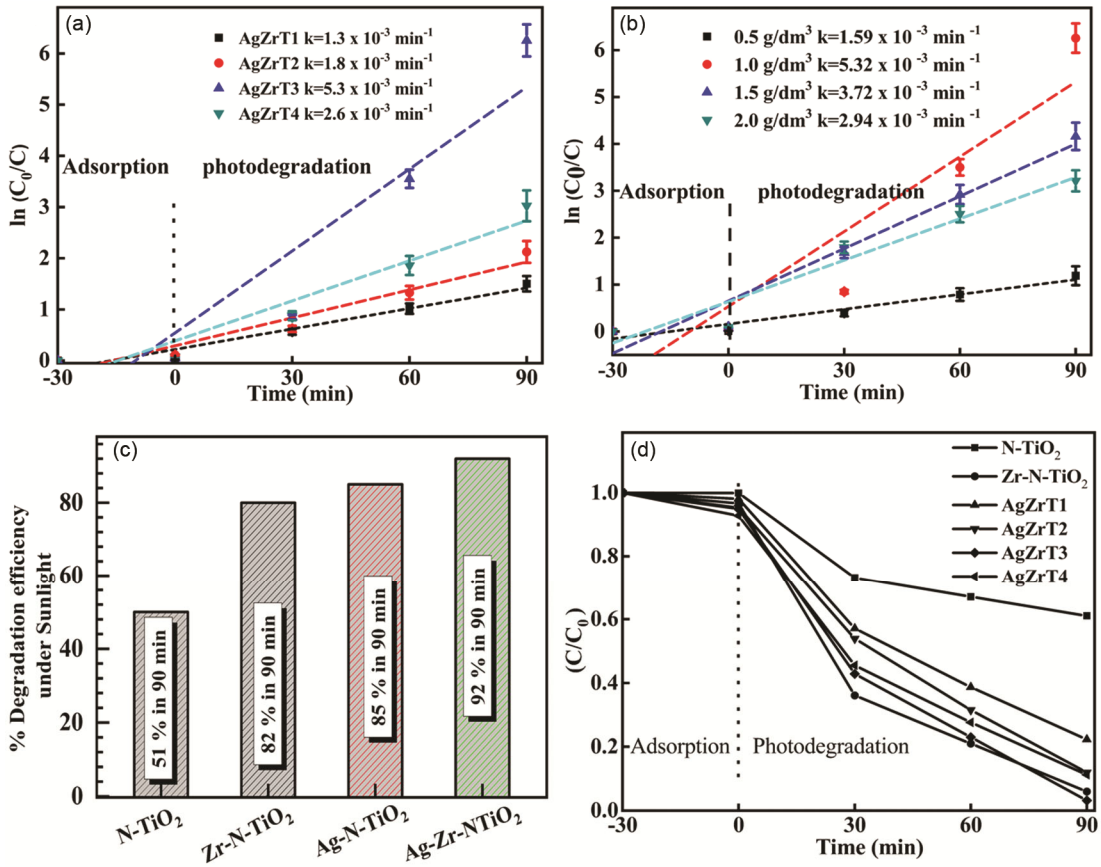


Fig. 5 — A) Kinetics study of effect of Ag content, B) Kinetics study of effect of catalyst loading and C) Comparison of photodegradation efficiencies of N-$TiO_2$, Zr-N-$TiO_2$ (Zr-0.5 mole%),Ag-N-$TiO_2$ (Ag-0.5 wt%),Ag-Zr-N-$TiO_2$ (Ag-0.5 wt% and Zr-0.5 mole%) against photodegradation of MO and D) Comparison of photodegradation efficiencies of AgZrT NCs with N-$TiO_2$ and Zr-N-$TiO_2$

$1.3\times10^{-3}$ to $5.3\times10^{-3}$ $min^{-1}$ and then decreases for 0.75 wt % of Ag in Zr-N-$TiO_2$. The highest rate constant was observed for 0.5 wt% of Ag and this composition was selected as optimal Ag loading. Improvement in the photocatalytic activity was witnessed due to increased light absorptivity by a narrow band gap material, induced defects *via* the doping of impurities into $TiO_2$ lattice and synergistic effect between Ag and Zr[32].

**Effect of catalyst loading**

The experimental amount of catalyst (NCs) was changed from 0.5 to 2.0 g/$dm^3$ by keeping other experimental parameters identical to get optimized catalyst amount. Investigation of catalyst loading was done by plotting ln($C_0$/C) against time (t). Fig. 5B indicates that the photodegradation of MO dye using AgZrT NCs follows pseudo-first order kinetics. On increasing the amount of catalyst from 0.5 to 1.0 g /$dm^3$, the rate gradually increases from $1.59\times10^{-3}$ to $5.32\times10^{-3}$ $min^{-1}$ and then decreases to $2.94\times10^{-3}$ $min^{-1}$. The highest rate constant value is observed for 1.0 g/$dm^3$ catalyst loading and it is directly proportional to the number of adsorption active sites and the number of absorbed photons by the catalyst. The decreased degradation with increased catalyst amount is due to the increasing turbidity of the suspension[33]. This leads to scattering effects due to which the actual amount of incident light used by catalyst for photodegradation decreases as catalyst amount increases [34].However, the agglomeration causes the decrease in active sites on the catalyst surface and becomes unavailable for photon absorption.

**The MO dye degradation performance using N-$TiO_2$, Zr-$TiO_2$ and AgZrTNCs**

For better understanding of mechanism and optimization of Zr and Ag content, comparison of photocatalytic degradation of MO using different photocatalyst is studied. Plot of % degradation efficiency of catalyst under sunlight for different catalyst was plotted as shown in Fig. 5C. However, the

comparison of photodegradation efficiencies of obtained AgZrT NCs with N-$TiO_2$ and Zr doped N-$TiO_2$ is revealed in Fig. 5D. N-$TiO_2$ shows 51% degradation of MO while Zr-N-$TiO_2$ shows 82% degradation. The enhancement in photodegradation of MO was observed with increase in Ag loading from AgZrT1 to AgZrT3, however with increment in Ag content leads to decrement in photodegradation (AgZrT4). The AgZrT3 NC showed optimum photodegradation efficiency (92%) for MO in90 minutes.

**Effect of irradiation sources**

The effect of irradiation sources on photocatalytic performance of NCs was carried out under UV light and Sunlight. Fig. 6A shows absorption spectra of MO under UV light for sample AgZrT3 as optimized catalyst. The peak intensities at 464 nm and 270 nm begins to decrease slightly (adsorption-desorption equilibrium) and about 6% dye is adsorbed on photocatalyst. After 30 min., intensity of peak at 464 and 270 nm decreases due to the formation of $CO_2$ and $H_2O$ by degradation of aromatic rings of MO under UV light[35] and similar trend was observed in case of Sunlight irradiation (Fig. 6B).The degradation of dye occurs with no significant shift in the wavelength ($\lambda_{max}$) of MO and no extra peak in absorption spectra of timely drawn aliquots confirms absence of harmful toxic intermediate by products.

A Photocatalytic degradation study shows that, 99% and 92% of degradation was achieved under UV and sunlight within 90 min. In order to overcome various hazardous effects of UV light such as cancer-causing effect and acute chronic health effect and to lessen the cost of electricity and UV light itself, natural sunlight is recommended for further photocatalytic degradation. 92% MO photodegradation was achieved using AgZrT3 within 90 min under sunlight.

**Probable photocatalytic mechanism of AgZrTNCs.**

The light dependent activity of photocatalyst depends upon phase composition (% anatase to rutile in case of $TiO_2$), surface area to volume ratio, crystallite size, absorption properties, rate of $e^-/h^+$ recombination. A probable degradation mechanism for AgZrTNCs is discussed below and shown as pathway A and B (Fig. 6C), respectively.

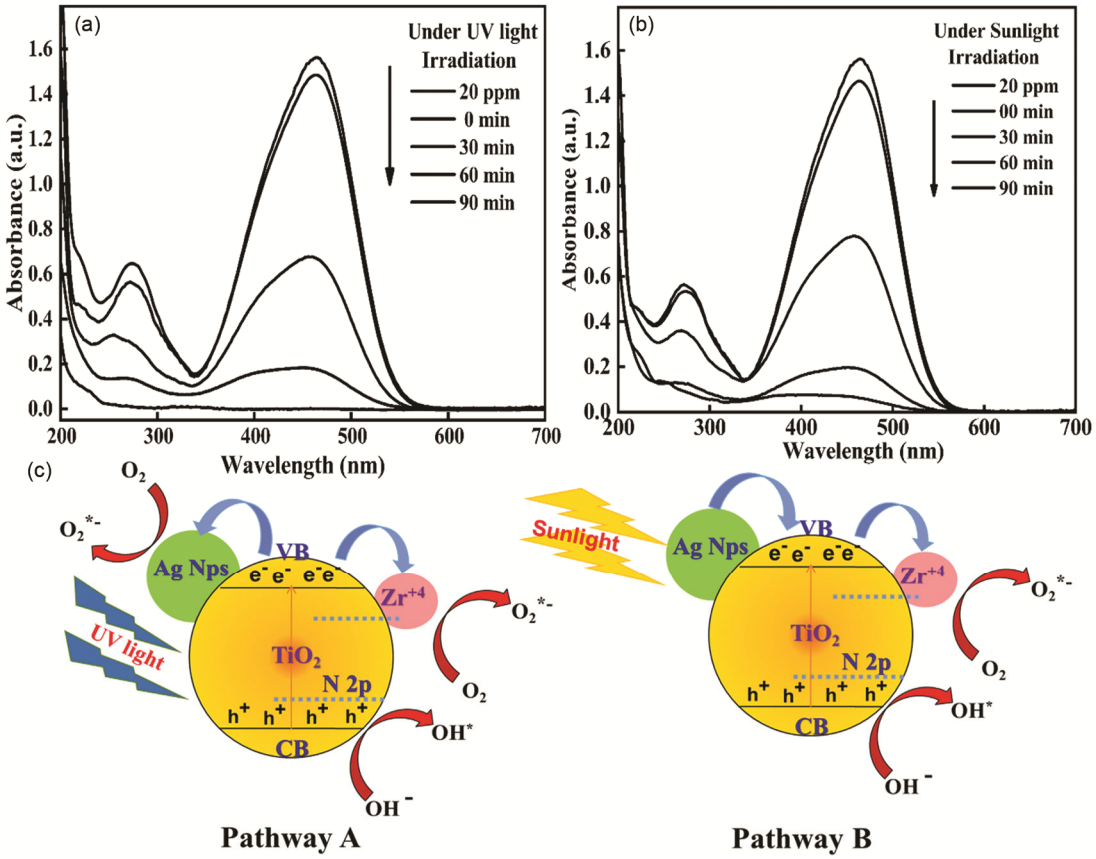


Fig. 6 — Effect of Irradiation sources on photodegradation of MO [20 ppm, catalyst dose =1.0 g/$dm^3$ of AgZrT3] in presence of A) UV B) Sunlight and C) Probable degradation mechanism of Ag loaded Zr doped N-$TiO_2$ NCs in presence of catalyst under UV light and Sunlight.

**Pathway A**

Previous report suggests that the microwave assisted method would be beneficial for NCs synthesis[22]. Upon UV light irradiation on AgZrT the photoelectrons generated in Valence Band, VB of $TiO_2$ get transferred to the Conduction Band, CB of $TiO_2$ leaving behind $h^+$ in VB. Although photoelectrons were generated from both VB of $TiO_2$ and localized N 2p level, but percentage of formation of photoelectrons in N 2p level was lesser compared to VB of $TiO_2$[36]. Fate of photoinduced carriers would decide the efficiency of photocatalyst, in case of AgZrT, the presence of Ag along with Zr helps to suppress photoelectron recombination rate by providing a competitive path for trapping of electrons. Transfer of trapped electron towards Ag was due to low work function of Ag compared to $TiO_2$ [37]. The combined action of Ag and Zr leads to the enhancement in photocatalytic efficiency.

**Pathway B**

Enhancement in the light dependent catalytic activity of AgZrTNCs in the presence of sunlight is due to the synergistic action of both Ag and Zr. In case of irradiation under sunlight, the SPR of Ag NPs plays an important role. The excited electrons generated in Ag NPs get transferred to CB of $TiO_2$, while Zr would act as an electron trap center. Due to the consortium action of SPR of Ag NPs and Zr trap centers, photocatalytic efficiency of AgZrT gets enhanced. In case of UV light and sunlight photoinduced $e^-$ and $h^+$ combine with adsorbed oxygen ($O_2$) and hydroxyl ion ($OH^-$) to generate superoxide radicals [$O_2^{-*}$] and hydroxyl radicals ($OH^*$) respectively which are accountable for the degradation of dye.

Overall, the increased performance of AgZrT at optimal Ag content against MO as model pollutant dye is due to synergic effect of Zr and N which help to create impurity dopant level in CB and VB of base material $TiO_2$, conversely the presence of Ag on the surface of ZrT which helps for shifting of absorbance spectra of fabricated material in visible region and both these effects in consortium enhances the photoactivity in solar region.

The explanation for photocatalysis pathways and identification of degradation products of MO are important to understand their fate. Hence, we have carried out the analysis of photodegraded product of MO using LC-MS and investigated the intermediates and probable route for the fragmentation of MO as shown in Fig. 7. The degradation reactions mainly contain the breaking of the C-N, C-S, O-S bonds. The molecular ion peak at m/z 304 corresponds to MO[M-H]$^{-}$[38], further, the MO fragments with loss of one –$CH_3$ group that gives the intermediate at m/z 290. After complete demethylation, there would be formation of intermediate having m/z at 276. The breaking of MO molecule is suggested by the presence of peaks at m/z 304, 290, 276, 240, 200,

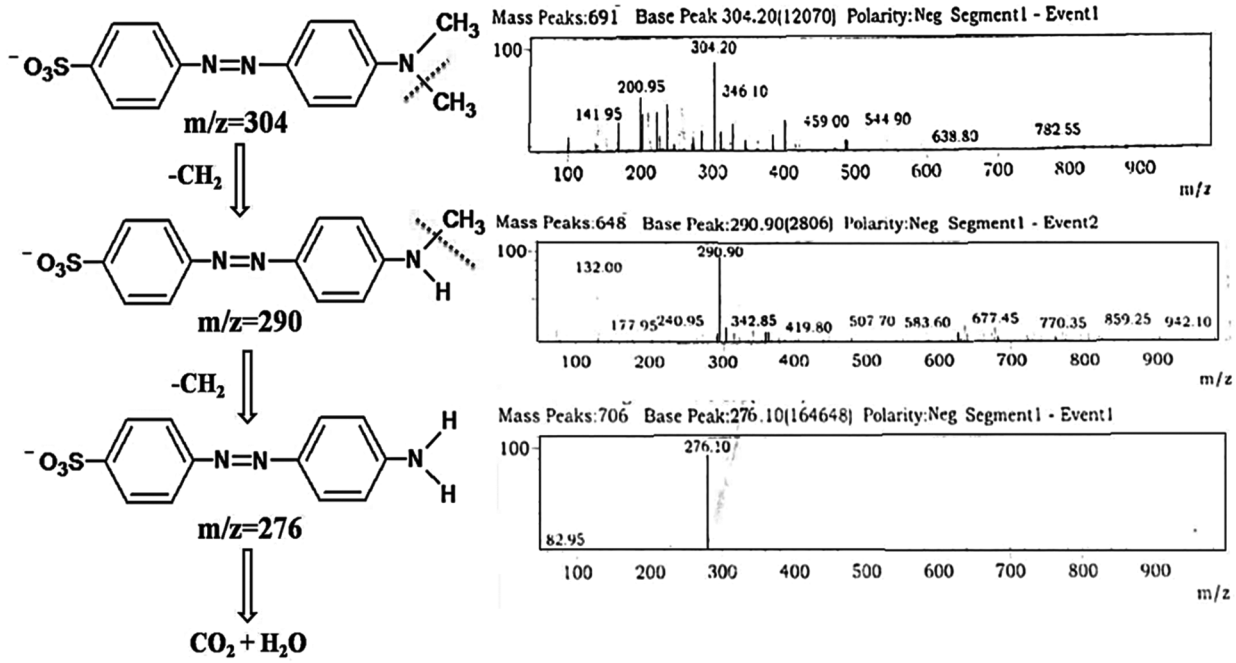


Fig. 7 — The proposed degradation pathway and LC-MS profile of methyl orange dye

177, 132 and 82. The products at m/z 276 and 290 are generated by homolytic cleavage of the N-C bond, which leads to the replaceable substitution of the -$CH_3$ group by the H atom[39].

## Conclusions

The present experimental work demonstrates the fabrication of Zr doped N-$TiO_2$ in anatase form by using simple and low cost-operative microwave technique. The impregnation and its subsequent reduction were utilized for further loading of Ag NPs on Zr-N$TiO_2$ in order to reduce the recombination of $e^-/h^+$ pairs. The UV data showed the shifting of absorption edge in the visible region due to consortium effect of both Ag and Zr. The crystallite size of fabricated NCs was in the range of 8 to 10 nm with anatase phase. EDS mapping with XPS data signifies presence of N, Zr, Ti and Ag along with oxygen deficiency that enhances photoactivity under UV and Sunlight. MO photodegradation using AgZrT NCs showed pseudo first order kinetics at 1.0 g/$dm^3$catalyst loading. Finally, it is concluded that Ag NPs loading tunes the UV active ZrT catalyst into Sunlight active AgZrT photocatalyst which efficiently degrades 92% MO within 90 min (0.5 wt % Ag). The synergistic action of SPR of Ag NPs and Zr trap centers are responsible for photocatalytic efficiency of AgZrT NCs under Sunlight.

## Acknowledgment

Authors are grateful to the Department of Science & Technology and Department of Biotechnology, New Delhi, for the grants under DST-FIST program (No. SR/FST/college-151/2013 (C)) and DBT-Star College Scheme to Jaysingpur College, Jaysingpur.

## References

1 Navya P N & Daima H K, *Nano Conver*, 3 (2016) 1.
2 Lazar M A, Varghese S & Nair S S, *Catalysts*, 2 (2012) 572.
3 Paz Y, *App Cat B Env*, 99 (2010) 448.
4 Brar S K, Verma M., Tyagi R D & Surampalli R Y, *Waste Management*, 30 (2010) 504.
5 Li J, Ji J, Chen J & Zhang W, *J Nanopar Res*, 22 (2020) 224.
6 Nsude H E, Nsude K U, Whyte G M, Obodo R M, Iroegbu C, Maaza M & Ezema F I, *J Nanopar Res*, 22 (2020 )352.
7 Natarajan T S, & Tayade R J, *J Nanopar Res*, 23 (2021) 127.
8 Dahl M, Liu Y & Yin Y, *Chem Rev*, 114 (2014) 9853.
9 Kamble R J, Gaikwad P V, Garadkar K M, Sabale S R, Puri V R & Mahajan S S, *J Iranian Chem Soc*, 19 (2022) 303.
10 Saeed K, Sadiq M, Khan I, Ullah S, Ali N & Khan A, *App Water Sci*, 8 (2018) 60.
11 Gaikwad P, Sabale S, Kurane R, Kakade B, Parase H, Dhabbe R & Kamble P, *Inorg Nano-Metal Chem*, 53 (2023) 52.
12 Gawade V V, Sabale S R, Dhabbe R S & Garadkar K M, (2023). *J Mat Sci Mat Elec*, 34 (2023) 138.
13 Zhang J, Wu Y, Xing M, Leghari S A K & Sajjad S, *Energy & Env Sci*, 3 (2010) 715.
14 Hashimoto K, Irie H & Fujishima A, *Japanese J App Phy*, 44 (2005) 8269.
15 Yu J, Qi L & Jaroniec M, *J Phy Chem C*, 114 (2010) 13118.
16 Bae E & Choi W, *Environ Sci Technol*, 37 (2003) 147.
17 Huo Y, Bian Z, Zhang X, Jin Y, Zhu J & Li H, *J Phy Chem C*, 112 (2008) 6546.
18 Li H, Bian Z, Zhu J, Huo Y, Li H & Lu Y, *J Amer Chem Soc*, 129 (2007) 4538.
19 Aqeel M, Ikram M, Imran M, Ul-Hamid A, Qumar U, Shahbaz A & Saeed A, *RSC Advances*, 10 (2020) 42235.
20 Juma A, Acik I O, Oluwabi A T, Mere A, Mikli V, Danilson M & Krunks M, *Appl Surface Sci*, 387 (2016) 539.
21 Ilkhechi N N & Kaleji B K, *Opt Quantum Electron*, 48 (2016) 347.
22 Dhabbe R, Kadam A, Korake P, Kokate M, Waghmare P & Garadkar K, *J Mat Sci Mat Elec*, 26 (2015) 554.
23 Tian G, Chen Y, Pan K, Wang D, Zhou W, Ren Z & Fu H, *App Surf Sci*, 256 (2010) 3740.
24 Cheng X, Yu X & Xing Z, *App Surf Sci*, 258 (2012) 3244.
25 Yang Y, Wen J, Wei J, Xiong R, Shi J & Pan C, *ACS App Mat Interfaces*, 5 (2013) 6201.
26 Shirke B S, Korake P V, Hankare P P, Bamane S R & Garadkar KM, *J Mat Sci Mat Elec*, 22 (2011) 821.
27 Sanjinés R, Tang H, Berger H, Gozzo F, Margaritondo G & Lévy F, *J App Phy*, 75 (1994) 2945.
28 Pisarek M, Krawczyk M, Hołdyński M & Lisowski W, *ACS Omega*, 5 (2020) 8647.
29 Ren C, Yang B, Wu M, Xu J, Fu Z, lv Y, Guo T, Zhao Y & Zhu C, *J Haz Mat*, 182 (2010) 123.
30 Kadam A N, Dhabbe R S, Kokate M R, Gaikwad Y B & Garadkar K M, *Spectrochi Acta Part A Mol Biomol Spec*, 133 (2014) 669.
31 Mahadwad O K, Parikh P A, Jasra R V & Patil C, *Bull Mat Sci*, 34 (2011) 551.
32 Pardeshi S K & Patil A B, *Solar Energy*, 82 (2008) 700.
33 Kansal S K, Kaur N & Singh S, *Nanoscale Res Lett*, 4 (2009) 709.
34 Gnanaprakasam A, Sivakumar V M & Thirumarimurugan M, *Indian J Mat Sci*, 2015 (2015) 601827.
35 Lee H, Park Y-K, Kim S-J, Kim B H, Yoon, H-S & Jung S-C, *J Ind Eng Chem*, 35 (2016) 205.
36 Wang J, Tafen D N, Lewis J P, Hong Z, Manivannan A, Zhi M, Li M & Wu, N, *J Amer Chem Soc*, 131 (2009) 12290.
37 Moafi H F, Shojaie A F & Zanjanchi M A, *J Appl Polym Sci*, 127 (2013) 3778.
38 He Y, Grieser F & Ashokkumar M, *Ultrason Sonochem*, 18 (2011) 974.
39 Dvininov E, Joshi U A, Darwent J R., Claridge J B, Xu, Z, & Rosseinsky M J, *Chem Comm*, 47 (2011) 881.